

BEAM-BASED UNDULATOR FIELD CHARACTERIZATION AND CORRECTION AT DUV-FEL

H. Loos*, T. Shaftan,
BNL, Upton, NY 11973, USA

Abstract

We present the results of the commissioning of the 10 m long NISUS undulator of the Deep Ultra Violet Free Electron Laser (DUV-FEL) project. The magnet and diagnostics geometry is discussed and tolerances on the beam trajectory straightness are shown. The beam-based alignment algorithm and its application to correct the NISUS field errors are described.

DUV-FEL PROJECT

Up to date the Deep Ultra Violet Free Electron Laser (DUV-FEL) project is fully commissioned at the NSLS (BNL) [7]. The magnetic system of the FEL includes the 10 m long permanent magnet hybrid undulator NISUS [5] with 3.89 cm period length and 0.31 T peak field at 2.08 cm gap. The NISUS undulator consists of 16 sections with 32 poles in each. The six poles in the middle of every section are alternatingly canted with a cant angle of 0.108 rad. Additional magnetic fields can be superimposed onto the static magnetic undulator fields by means of a so-called 4-wire structure in every section consisting of 4 independently powered wires, which allows for any combination of vertical and horizontal dipole as well as normal and skew quadrupole fields. These coils are integrated within the vacuum chamber for the electron beam. Additional horizontal correction is provided by so-called pancake coils, which have a rather uniform dipole field within the gap.

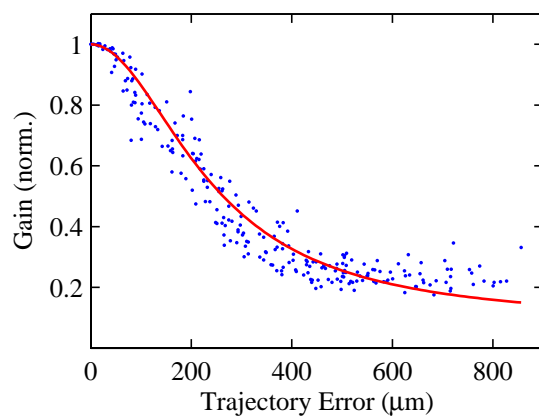


Figure 1: Gain reduction in NISUS for SASE at 266 nm due to rms trajectory deviation from field errors simulated with GENESIS 1.3. An empirical fit is shown in red.

*loos@bnl.gov

Along NISUS are 16 retractable YAG monitors [8] each with a periscope and image relay to an attached CCD camera. Two additional monitors 1 m and 6 cm in front of the wiggler are included to record the initial conditions of the electron beam with respect to the undulator. A HeNe laser beam, aligned to apertures before and after the undulator, provides a reference position for each monitor. The monitors are calibrated individually and have a resolution of approximately 10 μm (rms). An automated procedure in the MATLAB/EPICS control system records electron and laser beam images to obtain beam centroid and size at every monitor location. From these data the beam emittance, Twiss parameters, and launching condition at the wiggler entrance can be determined and corrected with upstream magnets [9].

To determine the tolerances on trajectory straightness we used the GENESIS 1.3 code [10], assuming the actual NISUS design. Gain length values were calculated for the beam parameters used in the HGHG experiment of 266 nm wavelength, 350 A peak current, 3 μm emittance and $2 \cdot 10^{-4}$ relative energy spread. For the error model used in the simulation we assumed that every section of NISUS has an error field value which is distributed uniformly over the section length. Correlated trajectory deviations which correspond to betatron oscillations were inhibited by imposing appropriate constraints on the field errors. The relative efficiency reduction, i.e. gain length increase, is shown in Fig. 1. A 10% relative increase of the gain length is induced by a field error of 1 mT (rms) or a trajectory error of 100 μm .

UNDULATOR FIELD MODEL

The fixed and variable electromagnetic focusing in NISUS can be regarded as uniform along the wiggler, since the resulting betatron wavelength is much longer than the section length. The electron beam trajectory for the horizontal plane $x(z)$ and similar for the vertical is then determined by the differential equation

$$x'' + k^2 x = \frac{B_y(z)}{B\rho}, \quad (1)$$

where $B_y(z)$ is the error magnetic field and k the betatron wavenumber. The solution of this differential equation,

$$x(z) = x_0 \cos(kz) + \frac{x'_0}{k} \sin(kz) + \int_0^z dz' \frac{B_y(z')}{k B\rho} \sin(k(z-z')), \quad (2)$$

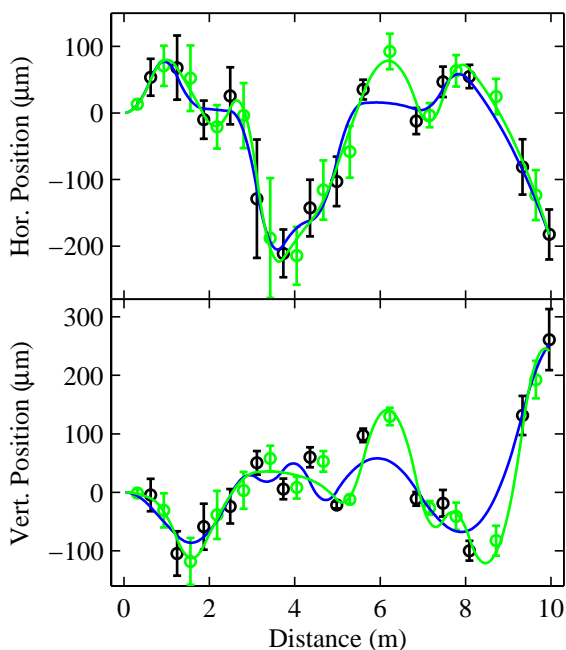


Figure 2: Horizontal and vertical beam position in NISUS with betatron oscillation removed. The green midpoints are obtained by quadratic interpolation. The solid curves represent the trajectories according to the field errors (Fig. 3) obtained from the linearly (blue) and quadratically (green) interpolated data.

contains two homogeneous terms, which correspond to non-zero initial conditions, and an inhomogeneous term caused by the field errors. The explicit solution of Eq. (2) depends on the field error model and can be integrated for uniform error fields B_i of length s_i centered within each section at location \bar{z}_i . For any trajectory propagating close enough to the undulator axis with small amplitude of betatron oscillation the focusing strength k in Eq. (1) can be neglected. The solution of this differential equation then gives at the monitor locations between consecutive sections for the inhomogeneous term

$$x_n^{\text{inh}} = \frac{1}{B\rho} \sum_{i=1}^n B_i s_i (z_n - \bar{z}_i). \quad (3)$$

This linear set of equations $x_n^{\text{inh}} = M_{ni} B_i$ can in principal be used to obtain the average field errors for each section from the measured beam positions. However, inspecting M reveals that it is badly conditioned and can not simply be inverted. Since there is no constraint for the trajectory angle at each monitor position, the trajectory obtained from the calculated field errors can have a large oscillation with a period of twice the section length. To avoid the oscillations, the trajectory angle can be constrained by introducing virtual monitors located between the real ones and interpolating the trajectory there with either a linear or a quadratic function.

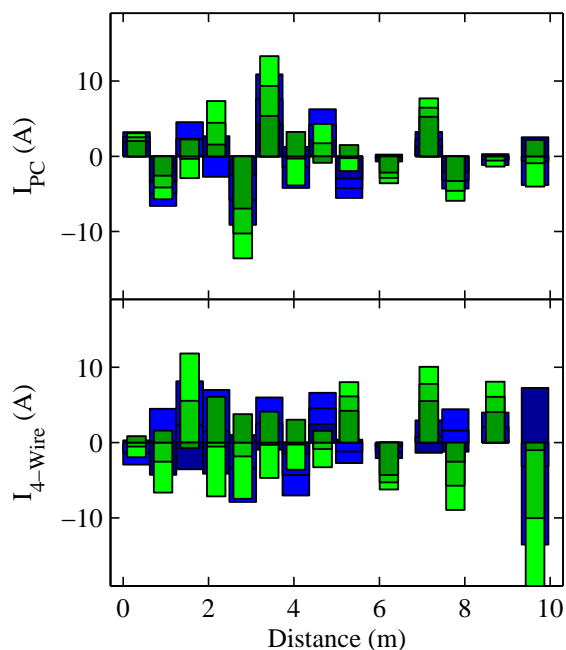


Figure 3: Correction currents for the trim coils required to compensate the calculated field errors from the linear (blue) and quadratic (green) model.

EXPERIMENTAL RESULTS

To determine the uncorrelated field errors, the pancake and 4-wire system was initially set to uniform values, which provide equal focusing strength and a magnetic axis at the reference laser position. Any remaining betatron oscillation from missteering at the undulator entrance was obtained by a fit to the data and subtracted to retrieve the trajectory corresponding to the inhomogeneous solution of Eq. (3). Figure 2 shows the uncorrelated trajectory deviation and the midpoints from quadratic interpolation (the midpoints in the linear case are not shown). The best fit of the field error distribution to the given beam positions are presented in Fig. 3 for both the linear and quadratic interpolation of the midpoints. The magnetic field is already scaled to corresponding trim corrector currents using $C_{\text{PC}} = 58 \mu\text{T/A}$ for the pancake correctors and $C_{4\text{W}} = 57 \mu\text{T/A}$ for the 4-wire trim coils. The two methods give very similar results. However, some of the calculated field errors are already dominated by the accuracy of the trajectory measurement, thus limiting the achievable precision of the correction discussed below.

Correcting the obtained field errors with corresponding changes in the trim coils and measuring the resulting trajectory, an iterative procedure was established to remove the field errors. The initial and final trajectory after three iterations can be seen in Fig. 4. The original trajectory deviation in respect to the betatron oscillation of $90 \mu\text{m}$ for both the horizontal and vertical direction was reduced to $38 \mu\text{m}$ and $29 \mu\text{m}$, respectively. The remaining deviation is comparable to the one of the reference laser, as shown in Fig. 5.

The displayed reference laser position is a single measurement in reference to the average over multiple scans, thus showing the reproducibility of the monitor positions and the jitter of the laser beam centroid. The iterative method converges within the precision of the trajectory measurement.

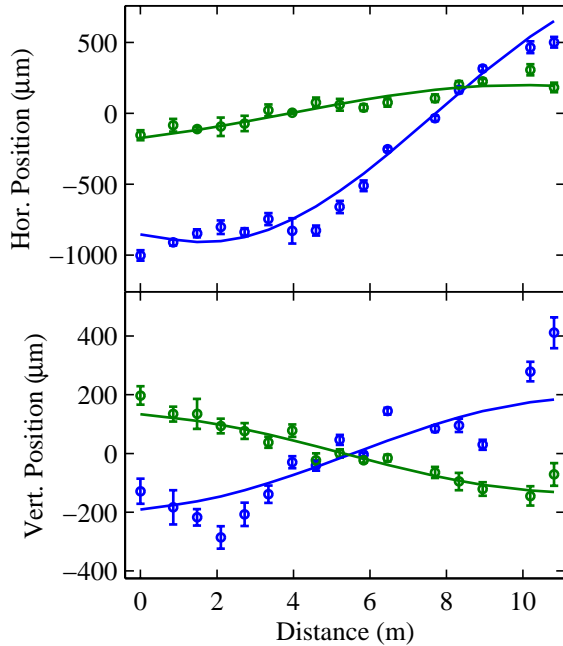


Figure 4: Initial (blue) and final (green) trajectory after three iterations of the correction algorithm.

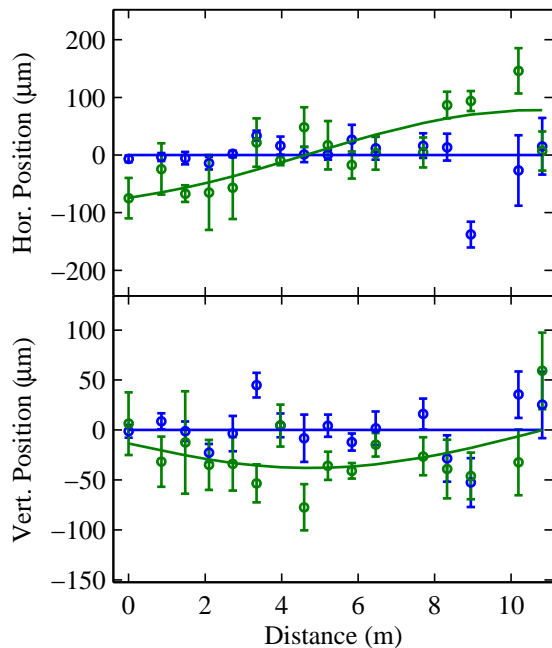


Figure 5: Final (blue) trajectory and reference laser position (green).

SUMMARY

The applicability of the BBA method presented here is demonstrated for the NISUS undulator. It is shown that for a complex undulator geometry including static and electromagnetic focusing a beam-based method works efficiently, providing electron beam parameters sufficient for a successful FEL performance.

ACKNOWLEDGEMENTS

The authors wish to thank L.-H. Yu and S. Krinsky for many fruitful discussions and A. Doyuran for his help with the diagnostics set-up and the experimental work. This activity was supported by DOE contract DEAC No. DE-AC02-98CH10886

REFERENCES

- [1] Ya. S. Derbenev, A. M. Konratenko, E. L. Saldin, Nucl. Instr. and Meth. A, **193** (1982) 415
- [2] L. H. Yu, S. Krinsky, R. L. Gluckstern, Phys. Rev. Lett. **64** (1990) 3011
- [3] L. H. Yu, S. Krinsky, R. L. Gluckstern, J. B. J. van Zeijts, Phys. Rev. A **45** (1992) 1163
- [4] P. Tenenbaum, T. O. Raubenheimer, Phys. Rev. ST Accel. Beams **3** (2000) 052801
- [5] D.C. Quimby *et al.*, Nucl. Instr. and Meth. A **285** (1989) 281
- [6] G. Rakowsky *et al.*, PAC 1999, New York, March 1999, p. 2698
- [7] T. Shaftan *et al.*, *First SASE and Seeded FEL Lasing of the NSLS DUV-FEL at 266 & 400 nm*, FEL 2002, Argonne, IL, September 2002
- [8] A. Doyuran *et al.*, *Diagnostics System for the NISUS Wiggler and FEL Observations at the BNL Source Development Lab*, EPAC 2002, Paris, June 2002, p. 802
- [9] H. Loos *et al.*, *Beam-based trajectory alignment in the NISUS wiggler*, EPAC 2002, Paris, June 2002, p. 837
- [10] S. Reiche, Nucl. Instrum. Meth. A **429** (1999) 243